a VTI model for layered unconventional reservoirs

Juan E. Santos [a,b,c,*]

[a] *Department of Mathematics, Purdue University, 150 N. University Street, West Lafayette, Indiana, 47907-2067, USA.*

[b] *Universidad de Buenos Aires, Facultad de Ingeniería, Instituto del Gas y del Petróleo, Av. Las Heras 2214 Piso 3 C1127AAR Buenos Aires, Argentina.*

[c] *Universidad Nacional de La Plata, La Plata, Argentina.*

---

[*] Corresponding author. E-mail address: santos@math.purdue.edu (J. E. Santos).

Abstract

BLA BLA

Keywords: Anisotropy, Layered Media, Two-phase Fluids, Poroelasticity, Effective Media.

1 The 2PBM describing a poroelastic solid saturated by a two-phase fluid

We consider a porous solid saturated by two immiscible fluids, where we distinguish a *wetting* phase and a *non-wetting* one, to be denoted with the subscripts (or superscripts) "w" and "n", respectively. Let $\mathbf{x} = (x, y, z)$ and $S_w = S_w(\mathbf{x})$ and $S_n = S_n(\mathbf{x})$ denote the wetting and non-wetting fluid saturations averaged over the bulk material, respectively, with S_{rw} and S_{rn} being the corresponding residual saturations. We assume that both fluid phases completely saturate the porous part and move within the pore space, [30,31], so that $S_w + S_n = 1.$ and $S_{rn} < S_n < 1 - S_{rw}$.

Denote by $\mathbf{u}^s = (u_i^s)$, $\widetilde{\mathbf{u}}^n = (\widetilde{u}_i^n)$ and $\widetilde{\mathbf{u}}^w = (\widetilde{u}_i^w)$, $i = 1, 2, 3$ the time Fourier transforms of the averaged displacement vectors of the solid, non-wetting and wetting phases, respectively, and let $\phi = \phi(\mathbf{x})$ denote the matrix effective porosity. The relative fluid displacements are

$$\mathbf{u}^\theta = \phi(\widetilde{\mathbf{u}}^\theta - \mathbf{u}^s),\ \xi^\theta = -\nabla \cdot \mathbf{u}^\theta,\ \theta = n, w.$$

Let $\varepsilon_{ij}(\mathbf{u}^s)$ and $e^s = \varepsilon_{ii}(\mathbf{u}^s)$ be the Fourier transforms of the strain tensor of the solid and its linear invariant, respectively. Also, set $\mathbf{u} = (\mathbf{u}^s, \mathbf{u}^n, \mathbf{u}^w)$.

Let $\boldsymbol{\tau} = \tau_{ij}$ and $\boldsymbol{\varepsilon} = \boldsymbol{\varepsilon}_{ij}$, $i, j = 1, 2, 3$ denote the Fourier transforms infinitesimal changes in the stress and strain tensors, respectively. Also, let P_n and P_w denote the Fourier transforms of the infinitesimal changes in the non-wetting and wetting fluid pressures, respectively. These infinitesimal changes are taken with respect to corresponding reference values $\bar{\tau}_{ij}$, $\bar{P}_n$, and $\bar{P}_w$ associated with the initial equilibrium state having non-wetting fluid saturation $\bar{S}_n$ and porosity $\bar{\phi}$. P_n and P_w are related through the capillary relation [30,31]

$$P_{ca} = P_{ca}(S_n + \bar{S}_n) = \bar{P}_n + P_n - (\bar{P}_w + P_w) = P_{ca}(\bar{S}_n) + P_n - P_w \geq 0. \quad (1)$$

Ignoring hysteresis, P_{ca} is a positive and strictly increasing function of the

non-wetting fluid saturation.

The stress-strain of a 2PBM are [27,29,23]:

$$\tau_{ij}(\mathbf{u}) = 2\mu\,\varepsilon_{ij} + \delta_{ij}(\lambda_c\, e^s - B_1\,\xi^n - B_2\,\xi^w), \tag{2}$$
$$\mathcal{T}_n(\mathbf{u}) = \left(\bar{S}_n + \beta + \zeta\right) P_n - (\beta + \zeta)\, P_w = -B_1\, e^s + M_1\,\xi^n + M_3\,\xi^w, \tag{3}$$
$$\mathcal{T}_w(\mathbf{u}) = \left(\bar{S}_w + \zeta\right)\, P_w - \zeta\, P_n = -B_2\, e^s + M_3\,\xi^n + M_2\,\xi^w, \tag{4}$$

where

$$\beta = \frac{P_{ca}(\overline{S}_n)}{P'_{ca}(\bar{S}_n)}, \zeta = \frac{\overline{P_w}}{P'_{ca}(\bar{S}_n)}. \tag{5}$$

The quantities τ_{ij}, $\mathcal{T}_n$ and $\mathcal{T}_w$ are the generalized forces of the system. The coefficient μ is the shear modulus of the dry rock, while $\lambda_c = K_c - \frac{2}{3}\mu$ with K_c being the undrained bulk modulus. The coefficients in (2)-(4) can be are determined as indicated in [27,29,23].

The equations for a 2PBM in the diffusive range of frequencies, stated in the space–frequency domain are [27,29,23]:

$$\nabla \cdot \boldsymbol{\tau}(\mathbf{u}) = 0, \tag{6}$$
$$i\omega\, d_n\, \mathbf{u}^n - i\omega\, d_{nw}\, \mathbf{u}^w + \nabla \mathcal{T}_n(\mathbf{u}) = 0, \tag{7}$$
$$i\omega\, d_w\, \mathbf{u}^w - i\omega\, d_{nw}\, \mathbf{u}^n + \nabla \mathcal{T}_w(\mathbf{u}) = 0. \tag{8}$$

The coefficients $d_n,\ d_w$ and d_{nw} are taken to be of the form:

$$d_l(\bar{S}_l) = (\bar{S}_l)^2 \frac{\eta_l}{\kappa K_{rl}(\bar{S}_l)}, \quad l = n, w, \tag{9}$$
$$d_{r,nw}(\bar{S}_n, \bar{S}_w) = \epsilon \left(d_n(\bar{S}_n) d_w(\bar{S}_w)\right). \tag{10}$$

Here η_n, η_w are the fluid viscosities and κ, $K_{rn}(S_n), K_{rw}(S_w)$ are the absolute permeability and the relative permeability functions, respectively, while $d_{r,nw}(S_n, S_w)$ is a cross dissipative function. In the numerical experiments we choose $\epsilon = 0.01$.

2 The equivalent TIV medium

Let us consider x_1 and x_3 as the horizontal and vertical coordinates, respectively. As shown in [15] a fluid-saturated poroelastic solid with a set of hori-

zontal layers behaves as a TIV medium with a vertical symmetry axis at long wavelengths.

Denote by $\tau_{ij}(\widetilde{\mathbf{u}}_s)$ and $\epsilon_{ij}(\widetilde{\mathbf{u}}_s)$ the stress and strain tensor components of the equivalent TIV medium, where $\widetilde{\mathbf{u}}_s$ denotes the solid displacement vector at the macroscale. The corresponding stress-strain relations, stated in the space-frequency domain and assuming a closed system are [32,8]

$$\tau_{11}(\widetilde{\mathbf{u}}_s) = p_{11}\ \epsilon_{11}(\widetilde{\mathbf{u}}_s) + p_{12}\ \epsilon_{22}(\widetilde{\mathbf{u}}_s) + p_{13}\ \epsilon_{33}(\widetilde{\mathbf{u}}_s), \tag{11}$$
$$\tau_{22}(\widetilde{\mathbf{u}}_s) = p_{12}\ \epsilon_{11}(\widetilde{\mathbf{u}}_s) + p_{11}\ \epsilon_{22}(\widetilde{\mathbf{u}}_s) + p_{13}\ \epsilon_{33}(\widetilde{\mathbf{u}}_s), \tag{12}$$
$$\tau_{33}(\widetilde{\mathbf{u}}_s) = p_{13}\ \epsilon_{11}(\widetilde{\mathbf{u}}_s) + p_{13}\ \epsilon_{22}(\widetilde{\mathbf{u}}_s) + p_{33}\ \epsilon_{33}(\widetilde{\mathbf{u}}_s), \tag{13}$$
$$\tau_{23}(\widetilde{\mathbf{u}}_s) = 2\ p_{55}\ \epsilon_{23}(\widetilde{\mathbf{u}}_s), \tag{14}$$
$$\tau_{13}(\widetilde{\mathbf{u}}_s) = 2\ p_{55}\ \epsilon_{13}(\widetilde{\mathbf{u}}_s), \tag{15}$$
$$\tau_{12}(\widetilde{\mathbf{u}}_s) = 2\ p_{66}\ \epsilon_{12}(\widetilde{\mathbf{u}}_s). \tag{16}$$

Note that in a TIV medium $p_{12} = p_{11} - 2\ p_{66}$, so that only five independent stiffness, i.e., $p_{11}, p_{33}, p_{13}, p_{55}$ and p_{66} need to be considered.

As shown in [21,22] these stiffnesses can be determined using five time-harmonic experiments. Next we present the generalization of those experiments using the 2PBM to determine a TIV medium long-wave equivalent to a fine layered poroelastic solid saturated by a two-phase fluid.

We will solve (6)-(8) in the 2D case on a reference square $\Omega = (0, L)^2$ with boundary Γ in the (x_1, x_3)-plane. Set $\Gamma = \Gamma^L \cup \Gamma^B \cup \Gamma^R \cup \Gamma^T$, where $\Gamma^L, \Gamma^R, \Gamma^B$ and Γ^T denote the left, right, bottom and top boundaries of Ω. Denote by $\boldsymbol{\nu}$ the unit outer normal on Γ and let $\boldsymbol{\chi}$ be a unit tangent on Γ oriented counterclockwise so that $\{\boldsymbol{\nu}, \boldsymbol{\chi}\}$ is an orthonormal system on Γ. To determine the five independent stiffness coefficients, we solve (6)-(8) in Ω with the boundary conditions

$$\mathbf{u}^n \cdot \boldsymbol{\nu} = 0, \quad \mathbf{u}^w \cdot \boldsymbol{\nu} = (x_1, x_3) \in \Gamma, \tag{17}$$

i.e., no fluids enter or leave the sample, and the additional boundary conditions:

for p_{33}:

$$\boldsymbol{\tau}(\mathbf{u})\nu \cdot \boldsymbol{\nu} = -\Delta P, \quad (x_1, x_3) \in \Gamma^T, \tag{18}$$
$$\boldsymbol{\tau}(\mathbf{u})\nu \cdot \boldsymbol{\chi} = 0, \quad (x_1, x_3) \in \Gamma, \tag{19}$$
$$\mathbf{u}^s \cdot \boldsymbol{\nu} = 0, \quad (x_1, x_3) \in \Gamma \setminus \Gamma^T. \tag{20}$$

Using the relation

$$\frac{\Delta V(\omega)}{V} = -\frac{\Delta P}{p_{33}(\omega)}, \tag{21}$$

where V the original volume of the sample, $p_{33}(\omega)$ can be determined from (21) measuring the complex volume change $\Delta V(\omega) \approx L u_{s,3}^{(33,T)}(\omega)$, where $u_{s,3}^{(33,T)}(\omega)$ is the average of the vertical component of the solid phase at the boundary Γ^T.

for p_{11}:

$$\boldsymbol{\tau}(\mathbf{u})\nu \cdot \boldsymbol{\nu} = -\Delta P, \quad (x_1, x_3) \in \Gamma^R, \tag{22}$$
$$\boldsymbol{\tau}(\mathbf{u})\nu \cdot \boldsymbol{\chi} = 0, \quad (x_1, x_3) \in \Gamma, \tag{23}$$
$$\mathbf{u}^s \cdot \boldsymbol{\nu} = 0, \quad (x_1, x_3) \in \Gamma \setminus \Gamma^R. \tag{24}$$

Thus, this experiment determines p_{11} as indicated for p_{33}, measuring the oscillatory volume change.

for p_{13}:

$$\boldsymbol{\tau}(\mathbf{u})\nu \cdot \boldsymbol{\nu} = -\Delta P, \quad (x_1, x_3) \in \Gamma^R \cup \Gamma^T, \tag{25}$$
$$\boldsymbol{\tau}(\mathbf{u})\nu \cdot \boldsymbol{\chi} = 0, \quad (x_1, x_3) \in \Gamma, \tag{26}$$
$$\mathbf{u}^s \cdot \boldsymbol{\nu} = 0, \quad (x_1, x_3) \in \Gamma^L \cup \Gamma^B. \tag{27}$$

From (11) and (13) we get

$$\sigma_{11} = p_{11}\epsilon_{11} + p_{13}\epsilon_{33} \quad \sigma_{33} = p_{13}\epsilon_{11} + p_{33}\epsilon_{33},$$

with ϵ_{11} and ϵ_{33} being the (macroscale) strain components at Γ^L and Γ^T, respectively. Since $\sigma_{11} = \sigma_{33} = -\Delta P$ (c.f.(25)) we obtain $p_{13}(\omega)$ as

$$p_{13}(\omega) = \frac{p_{11}\epsilon_{11} - p_{33}\epsilon_{33}}{\epsilon_{11} - \epsilon_{33}}. \tag{28}$$

for p_{55}:

$$-\boldsymbol{\tau}(\mathbf{u})\boldsymbol{\nu} = \mathbf{g}, \quad (x_1, x_3) \in \Gamma^T \cup \Gamma^L \cup \Gamma^R, \tag{29}$$
$$\mathbf{u}_s = 0, \quad (x_1, x_3) \in \Gamma^B, \tag{30}$$

where

$$\mathbf{g} = \begin{cases} (0, \Delta G), & (x_1, x_3) \in \Gamma^L, \\ (0, -\Delta G), & (x_1, x_3) \in \Gamma^R, \\ (-\Delta G, 0), & (x_1, x_3) \in \Gamma^T. \end{cases}$$

The change in shape of the rock sample allows to obtain $p_{55}(\omega)$ by using the relation

$$\mathrm{tg}(\beta\omega)) = \frac{\Delta G}{p_{55}(\omega)}, \tag{31}$$

where $\beta(\omega)$ is the departure angle between the original positions of the lateral boundaries and those after applying the shear stresses, that can be determined by measuring the average horizontal displacement at Γ^T [21,22].

for p_{66}:

$$-\boldsymbol{\tau}(\mathbf{u})\boldsymbol{\nu} = \mathbf{g}_2, \quad (x_1, x_2) \in \Gamma^B \cup \Gamma^R \cup \Gamma^T, \tag{32}$$

$$\mathbf{u}_s = 0, \quad (x_1, x_2) \in \Gamma^L, \tag{33}$$

where

$$\mathbf{g}_2 = \begin{cases} (\Delta G, 0), & (x_1, x_2) \in \Gamma^B, \\ (-\Delta G, 0), & (x_1, x_2) \in \Gamma^T, \\ (0, -\Delta G), & (x_1, x_2) \in \Gamma^R. \end{cases}$$

Then, we proceed as indicated for $p_{55}(\omega)$.

The approximate solution of these five BVP was computed using a FE procedure. We used bilinear functions to approximate each component of the solid displacement vector, while for the non-wetting and wetting fluid displacements we used a closed subspace of the vector part of the Raviart-Thomas-Nedelec space of zero order [33]. See [22,23] for details on the description of these finite element spaces. Also, it was shown in [22] that the error associated with these finite-element problems, measured in the energy norm, is on the order of $h^{1/2}$, with h being the size of the computational mesh. The proof can be generalized to the case of two-phase fluids analyzed here.

3 Numerical experiments

The FE procedures described above were implemented to determine the five complex stiffnesses $p_{IJ}(\omega)$ as a function of frequency. The corresponding phase and energy velocities and dissipation coefficients for qP, qSV and SH waves were computed as in [8].

In all the experiments the numerical samples are squares of side length 20 cm and were discretized using a 80×80 uniform mesh representing 10 periods of of 6 cm isotropic illite layers and 2 cm isotropic viscoleastic kerogen layers, with the layers saturated by two-phase fluids.

The saturant fluids were chosen to be two-phase mixtures of water-gas or oil-gas, with water being the wetting phase for the illite layers and oil being the wetting phase for the kerogen layers.

The grain bulk modulus, density, dry bulk and shear modulus, porosity and permeability of the illite are (in MKS units)

$$K_s = 28.43110^9 \quad \rho_s = 2700.0, \quad K_m = 18.0098 \times 10^9 \quad \mu_m = 12.4683 \times 10^9$$
$$\phi = 0.1, \quad \kappa = 2 \times 10^{-19}$$

For the kerogen layers, the grain density, dry bulk and shear modulus, porosity and permeability are (in MKS units)

$$K_s = 6.775910^9 \quad \rho_s = 1400.0, \quad K_m = 4.2923 \times 10^9 \quad \mu_m = 1.277 \times 10^9$$
$$\phi = 0.1, \quad \kappa = 2 \times 10^{-19}$$

The bulk modulus, density and viscosity of the fluids are 2.25 GPa, 1000 kg/m^3 and 0.001 Pa·s for water, 0.022 GPa, 78 Kg/m^3 and 0.00015 Pa·s for gas and 0.57 GPa, 700 Kg/m^3 and 0.01 Pa·s for oil, respectively.

In the illite layers, saturation for the water (wetting) phase is $S_w = 0.99$, while the nonwetting gas phase has saturation $S_g = 0.01$.

In the kerogen layers saturation for the wetting (oil) phase is $S_o = 0.05$, and the nonwetting gas phase has saturation is $S_g = 0.95$.

The two-phase fluid is described in terms of relative permeabilities, $K_{rn}(S_n)$, $K_{rw}(S_n)$, and capillary pressure function, $P_{ca}(S_n)$, taken to be [29,34]:

$$K_{rn}(S_n) = \left(1 - (1 - S_n)/(1 - S_{rn})\right)^2 ,$$
$$K_{rw}(S_n) = \left(\left[1 - S_n - S_{rw}\right] / \left(1 - S_{rw}\right)\right)^2 ,$$
$$P_{ca}(S_n) = A \left(1/(S_n + S_{rw} - 1)^2 - S_{rn}^2/[S_n(1 - S_{rn} - S_{rw})]^2\right) ,$$

where A is the capillary pressure amplitude, chosen to be 30 kPa in all experiments. These relations are based on laboratory experiments performed on different porous rocks during imbibition and drainage processes (neglecting

hysteresis effects) and are of common use in multiphase flow reservoir simulation.

The first experiment compares energy velocities and attenuation coefficients of qP, qSV, and SH waves for a two-phase gas-brine mixture defined using the 2PBM with those corresponding to the analytical solution using the SPBM as in [15], with the single-phase fluid determined by weighting the gas and brine properties with the corresponding saturations in background and fractures. Note that the analytical solution correspond to the case when the kerogen layers are *elastic*.

The effective single phase fluid viscosity $\eta^{(eff)}$, density $\rho^{(eff)}$ and bulk modulus $K^{(eff)}$ are computed as follows,

$$\begin{aligned}
\eta^{(eff)} &= \eta_n S_n + \eta_w S_w, \\
\rho^{(eff)} &= \rho_n S_n + \rho_w S_w \\
\frac{1}{K^{(eff)}} &= \frac{S_n}{K_n} + \frac{S_w}{K_w},
\end{aligned}$$

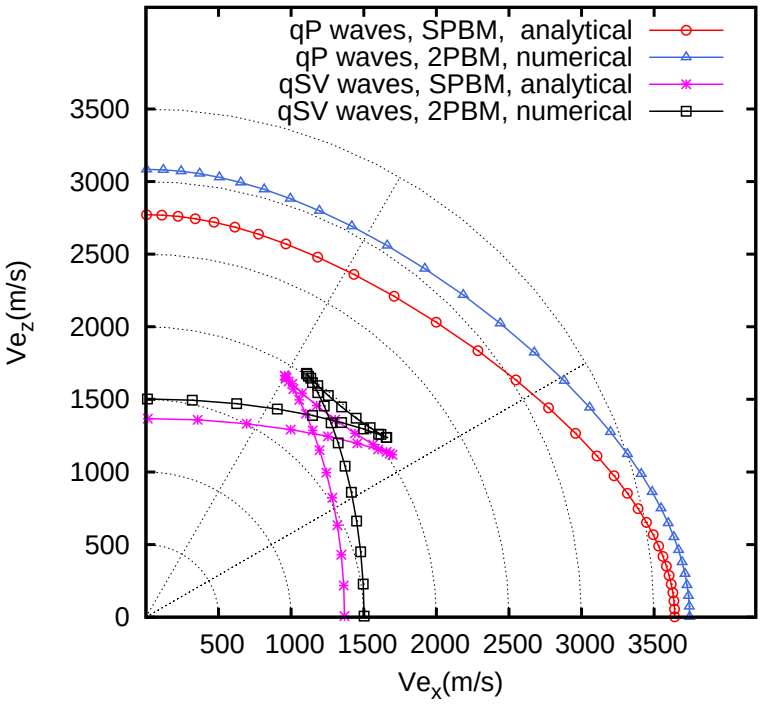

Fig. 1. Polar representation of energy velocities of qP and qSV waves of the 2PBM for a two-phase gas-brine fluid and those of the analytical model, the latter computed using and effective single-phase fluids. Residual saturations are $S_{rn} = 0, S_{rw} = 0.01$.

References

[1] Gurevich, B., Elastic properties of saturated porous rocks with aligned fractures, J. Appl. Geophys. (2003); 54: 203-218.

[2] Gurevich, B., Brajanovski, M., Galvin, R. J., Müller, T. M. and Toms-Stewart, J., P-wave dispersion and attenuation in fractured and porous reservoirs–poroelasticity approach, Geophys. Prospect. 2009; 57: 225-237.

[3] Biot, M. A., Theory of propagation of elastic waves in a fluid-saturated porous solid. I. Low frequency range, J. Acoust. Soc. Am. 1956a; 28: 168 – 178.

[4] Biot, M. A., Theory of propagation of elastic waves in a fluid-saturated porous solid. II. High frequency range, J. Acoust. Soc. Am. 1956b; 28: 179 – 191.

[5] Biot, M. A., Mechanics of deformation and acoustic propagation in porous media, *J. Appl. Phys.* 1962; 33: 1482 – 1498.

[6] Plona, T., Observation of a second bulk compressional wave in a porous medium at ultrasonic frequencies, Applied Physics Letters 1980; 36: 259-261.

[7] J. M. Carcione and S. Picotti, P-wave seismic attenuation by slow-wave diffusion, Effects of inhomogeneous rock properties, Geophysics 2006; 71: O1-O8.

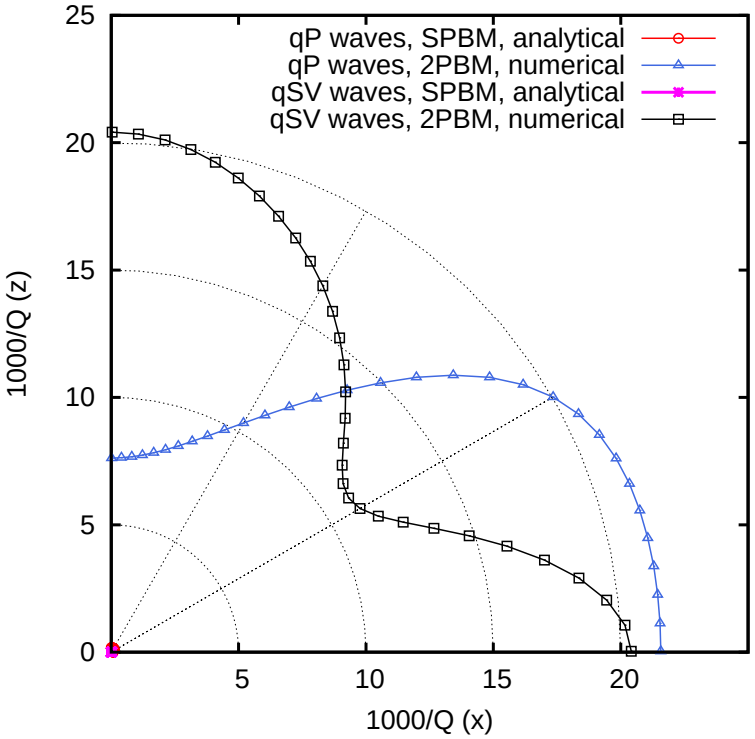

Fig. 2. Polar representation of attenuation coefficient of qP and qSV waves of the 2PBM for a two-phase gas-brine fluid and those of the analytical model, the latter computed using and effective single-phase fluids. Residual saturations are $S_{rn} = 0, S_{rw} = 0.01$.

[8] J. M. Carcione, Wave Fields in Real Media. Theory and numerical simulation of wave propagation in anisotropic, anelastic, porous and electromagnetic media, Elsevier. (Third edition, extended and revised), Oxford; 2015.

[9] J. E. White, N. G. Mikhaylova and F. M. Lyakhovitskiy, Low-frequency seismic waves in fluid saturated layered rocks, Physics of the Solid Earth 1975; 11: 654-659.

[10] N. C. Dutta, H. Odé, Attenuation and dispersion of compressional waves in fluid-filled porous rocks with partial gas saturation (White model). Part I: Biot theory, Geophysics 1979; 44 (11): 1777-1788.

[11] Mochizuki, S., Attenuation in partially saturated rocks, J. Geophys. Res.1982; 87: 8598-8604.

[12] Berryman, J., Thigpen, L. and Chin, R., Bulk elastic wave propagation in partially saturated porous solids, J. Acoust. Soc. Am. 1988; 84: 360–373.

[13] Carcione, J. M., Kosloff, D. and Behle, A., Long wave anisotropy in stratified media: a numerical test, Geophysics 1991; 56: 245-25.

[14] Gelinsky, S. and Shapiro, S. A., Poroelastic Backus-averaging for anisotropic, layered fluid and gas saturated sediments, Geophysics 1997; 62: 1867-1878.

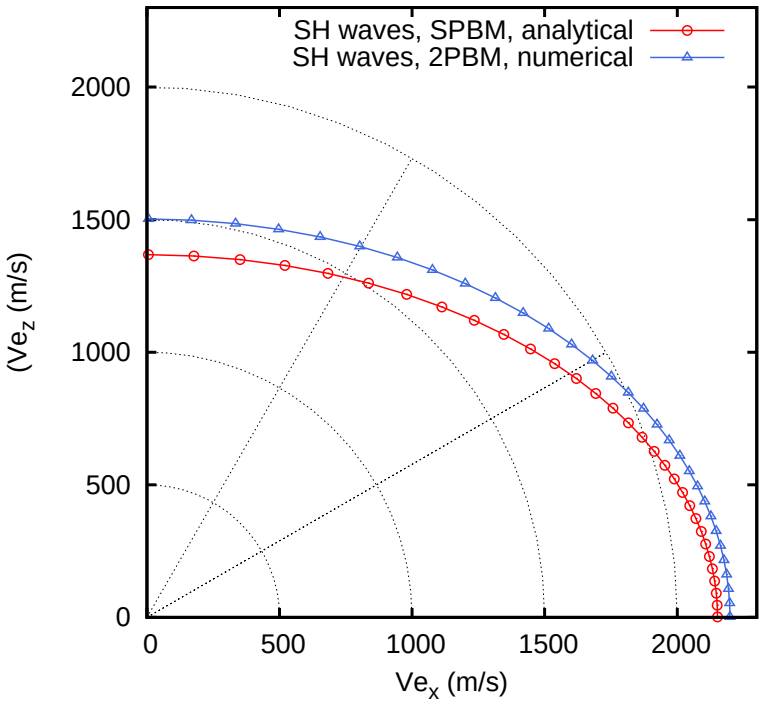

Fig. 3. Polar representation of energy velocities of SH waves of the 2PBM for a two-phase gas-brine fluid and those of the analytical solution, the latter computed using and effective single-phase fluids. Residual saturations are $S_{rn} = 0, S_{rw} = 0.01$.

[15] F. Krzikalla F. and Müller, T. M., Anisotropic P-SV-wave dispersion and attenuation due to interlayer flow in thinly layered porous rocks, Geophysics 2011; 76: WA135.

[16] Carcione, J. M., Gurevich, B., Santos, J. E., and Picotti, S., Angular and frequency dependent wave velocity and attenuation in fractured porous media, Pure and Applied Geophysics, 170, 1673-1683, 2013.

[17] Saenger E. H., Ciz, R., O. S. Krüger, O. S., Schmalholz, S. M., Gurevich, B., and Shapiro, S. A., Finite-difference modeling of wave propagation on microscale: A snapshot of the work in progress, Geophysics 2007; 72: SM293-SM300.

[18] Grechka, V. and M. Kachanov, M., Effective elasticity of rocks with closely spaced and intersecting cracks, Geophysics 2006; 71: D85D91.

[19] Wenzlau, F., Altmann, J. B. and Müller, T. M., Anisotropic dispersion and attenuation due to wave-induced flow: quasi-static finite element modeling in poroelastic solids, J. Geophys. Res. 2010; 115: B07204.

[20] Quintal, B. H., Steeb, M., Frehner, M. and Schmalholz, S. M., Quasi-static finite element modeling of seismic attenuation and dispersion due to wave-induced fluid flow in poroelastic media, J. Geophys. Res. 2011; 116: B01201.

[21] Santos, J. E., Martínez Corredor, R. and Carcione, J. M., Seismic velocity

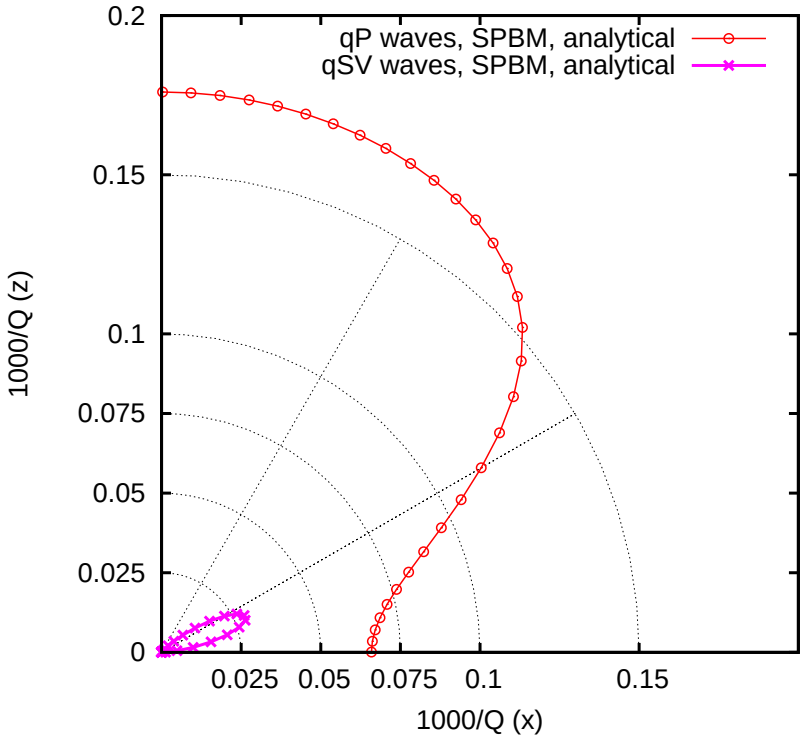

Fig. 4. Polar representation of attenuation coefficient of qP and qSV waves for the analytical solution computed using and effective single-phase fluids. Jose: aqui se grafican separados los casos analiticos de atenuacion de la Figura 2 porque los valores se ven como un punto en ese grafico.

and Q anisotropy in fractured poroelastic media, Int. J. Rock. Mech. Min. Sci. 2014; 70: 212 – 218.

[22] Santos, J. E. and Carcione, J. M., Finite-element harmonic experiments to model fractured induced anisotropy in poroelastic media, Comput. Methods Appl. Mech. Engrg. 2015; 283: 1189 – 1213.

[23] Santos, J. E. and Gauzellino, P. M. Numerical Simulation in Applied Geophysics, Birkhauser, Lecture Notes in Geosystems Mathematics and Computing, 2017.

[24] Auriault, J. L., Lebaigue, O. and Bonnet, G., Dynamics of two immiscible fluids flowing through deformable porous media, Transport in Porous Media 1989; 4: 105 – 128.

[25] Lo, W. C., Sposito, G. and Majer, E., Wave propagation through elastic porous media containing two immiscible fluids, Water Resources Research 2005; 41: W02025, 1-20.

[26] Qi., Q, Muller, T. M., Gurevich, B., Lopes, S., Lebedev, M., and Caspari, E., Quantifying the effect of capillarity on attenuation and dispersion in patchy-saturated rocks, Geophysics 2014; 79: WB35 WB50.

[27] Santos, J. E., Douglas, J., Jr., Corberó, J. and Lovera, O. M., A model for wave

propagation in a porous medium saturated by a two-phase fluid, J. Acoust. Soc. Am. 1990a; 87: 1439 – 1448.

[28] Santos, J. E., Corberó, J. M. and Douglas, J, Jr., Static and dynamic behaviour of a porous solid saturated by a two-phase fluid, J. Acoust. Soc. Am. 1990b; 87: 1428 – 1438.

[29] Ravazzoli, C. L., Santos, J. E. and Carcione, J. M., Acoustic and mechanical response of reservoir rocks under variable saturation and effective pressure, J. Acoust. Soc. Am., 2003; 113: 1801 – 1811.

[30] Scheidegger, A. E., The physics of flow through porous media, University of Toronto, Toronto, 1974.

[31] Peaceman, D. W., Fundamentals of numerical reservoir simulation, Elsevier, 1977.

[32] J. M. Carcione, Anisotropic Q and velocity dispersion of finely layered media. Geophys. Prosp. 1992; 40: 761-783.

[33] Raviart, P. A., and Thomas, J. M., Mixed finite element method for 2nd order elliptic problems, Mathematical Aspects of the Finite Element Methods, Lecture Notes of Mathematics, vol. 606, Springer, 1975.

[34] Douglas, J., Jr., Furtado, F. and Pereira, F., On the numerical simulation of waterflooding of heterogeneous petroleum reservoirs, Comput. Geosci. 1997; 1: 155 – 190.